Reachability Analysis of Low-Thrust, Cislunar Spacecraft using State-Transition Tensors

Ethan Foss
Stanford University

Aaron J. Rosengren
University of California San Diego

Ashley D. Biria
Air Force Research Laboratory

ABSTRACT

As presence in cislunar space expands, new methods for characterizing the capabilities of low-thrust spacecraft in the regions beyond geosynchronous orbit (GEO) are becoming more important. Spacecraft reachability analysis, which refers to the determination of the set of states that a spacecraft can travel to or come from using its propulsion system over a given amount of time, is fundamental to our understanding of spacecraft trajectories and their neighboring phase-space regions in this new dynamical topography. Reachability analysis offers multi-faceted utility to the space situational awareness community for tracking, detection, maneuver reconstruction, and evaluation of collision probabilities. However, the computation of reachable sets is a particularly formidable problem in astrodynamics and few methods exist to accurately and rapidly compute reachable sets for low-thrust spacecraft. Furthermore, computing reachable sets in the xGEO (beyond GEO) regime presents unique challenges due to the highly sensitive and chaotic dynamics environment. In this paper, we present a unique technique for propagating the reachable sets of low-thrust spacecraft in the cislunar environment that leverages state-transition tensors and set-based computing techniques.

1. INTRODUCTION

Growing international interest in cislunar missions beyond the geosynchronous belt (xGEO) necessitates enhanced tools and algorithms for space situational awareness (SSA) in order to facilitate safe and cooperative expansion into this multi-body regime. This requires the ability to evaluate collision probabilities, propagate uncertainty, characterize mission capabilities, and track spacecraft. Simultaneous to increasing cislunar interest is a push towards the use of electric propulsion (EP) for driving spacecraft missions. As space exploration moves towards these novel frontiers, new techniques must be adapted and developed.

Spacecraft reachability analysis refers to the set of states that a spacecraft can travel to or come from using its propulsion system over a given amount of time. It offers multifaceted utility for the aforementioned SSA capabilities, ensuring safety of missions, and path planning and control. However, evaluating the reachable sets of low-thrust spacecraft is a notoriously difficult problem owing to the fact that these spacecraft are continuously thrusting. Moreover, the highly nonlinear and chaotic environment that characterizes cislunar multi-body space renders the evaluation of reachable sets an endeavor fraught with considerable difficulty.

Reachability analysis is a classical problem in dynamical and controls systems for system verification, invariant-set computation, observation, and set-based prediction. It has been shown that the reachability problem is undecidable with even the simplest of dynamical systems [2], meaning there exists no algorithm that can solve the reachability problem correctly for most dynamical systems. Therefore, reachability analysis techniques require some form of approximation in order to reframe the problem in a manner that is computationally feasible. There are several means of computing reachable sets, however the three main categories involve: 1. solving an associated Hamilton-Jacobi-Bellman partial differential equation (HJB PDE) for propagating zero-sublevel sets; 2. random sampling integration of a large number of points; and 3. directly propagating reachable sets through set-based computing.

Approved for public release; distribution is unlimited. Public Affairs release approval #AFRL20244796.

The most popular approach that has seen success for low-thrust, cislunar spacecraft, involves random sampling and the propagation of a large number of trajectories. For example, [8] proposes a technique that leverages the indirect method of trajectory optimization by solving many optimal-control problems with a randomly sampled objectives. This technique produces a large number of extremal trajectories that outline the boundary of the reachable set in relevant directions. An adaptation of this technique is outlined in [15], whereby each optimal-control problem is suboptimally solved to improve computation time. Recently, [13] showed that generating extremal trajectories does not require solving an optimal-control problem and can be done simply by solving an ODE. However, this technique does not allow for sampling of extremal trajectories in specific spaces, such as the position or velocity space. All of these techniques suffer from the fact that they require a large number of trajectories to produce a good outline of the boundary of the reachable set. Moreover, these techniques can only provide mathematical guarantees on the convex hull of the reachable set, and therefore can struggle to produce good samples of non-convex reachable sets. Lastly, for those systems that demand a considerable expenditure of computational resources, such as realistic ephemeris models, this approach can be slow as it necessitates the resolution of numerous trajectories.

In this paper, we propose a novel approach to reachability analysis of low-thrust, cislunar spacecraft that leverages state-transition tensors and set-based computing to directly propagate reachable sets. Set-based reachability analysis, which uses set representations like polytopes, zonotopes, Taylor models, and polynomial zonotopes, is a popular method for performing reachability analysis among the cyberphysical systems community. However, such a technique for reachability analysis has not been demonstrated for the purposes of cislunar SSA. Moreover, typical implementations of set-based reachability computing use inaccurate means of discretization. By leveraging state-transition tensors, which have become popular for many astrodynamics applications like uncertainty propagation and optimal control, higher accuracy non-convex approximations of reachable sets can be obtained. Additionally, only one numerical integration need be performed, in contrast to other algorithms where numerous numerical integrations are required. We show how the proposed method performs in comparison to a selection of previously proposed methods for reachability set computation for distant retrograde orbits (DROs) in the circular, restricted, three-body problem (CR3BP). We then show how the method can be easily extended for higher-fidelity, reachable-set computation using ephemeris models of a cislunar spacecraft in a near-rectilinear halo orbit (NRHO).

2. BACKGROUND AND METHODOLOGY

2.1 Reachability

In this paper, the characterization of reachable sets under bounded time and bounded continuous time inputs is of interest. The reachable set at time t from some initial set $\mathcal{X}_0$ and input constraints $\mathcal{U}$ is defined as

$$\mathcal{R}(t) \triangleq \left\{ \boldsymbol{x}_0 + \int_{t_0}^{t} \boldsymbol{f}(\boldsymbol{x}(\tau), \boldsymbol{u}(\tau), \tau) \mathrm{d}\tau \mid \boldsymbol{x}_0 \in \mathcal{X}_0, \boldsymbol{u}(\tau) \in \mathcal{U} \; \forall \tau \in [t_0, t] \right\}. \tag{1}$$

Moreover, the reachable tube of the system is defined as

$$\mathcal{R}([t_0, t]) \triangleq \bigcup_{\tau \in [t_0, t]} \mathcal{R}(\tau). \tag{2}$$

Lastly, we define an extremal trajectory $\bar{\boldsymbol{x}}(t)$ as a feasible trajectory that lies on the boundary of the reachable set; i.e.,

$$\bar{\boldsymbol{x}}(t) \in \partial \mathcal{R}(t), \exists \boldsymbol{u}(t) \in \mathcal{U} \text{ s.t. } \dot{\bar{\boldsymbol{x}}}(t) = \boldsymbol{f}(\bar{\boldsymbol{x}}(t), \boldsymbol{u}(t), t) \; \forall t. \tag{3}$$

As is shown in [13], extremal trajectories can be generated by solving the following state-costate ODE:

$$\begin{aligned}
\begin{bmatrix} \dot{\boldsymbol{x}}(t) \\ \dot{\boldsymbol{\lambda}}(t) \end{bmatrix} &= \begin{bmatrix} \boldsymbol{f}(\boldsymbol{x}(t), \boldsymbol{u}^*(t), t) \\ -\left(\frac{\partial \boldsymbol{f}}{\partial \boldsymbol{x}} \big|_{\boldsymbol{x}(t), \boldsymbol{u}^*(t), t} \right)^{\mathsf{T}} \boldsymbol{\lambda}(t) \end{bmatrix} \quad \forall t \in [t_0, t_f], \\
\boldsymbol{u}^*(t) &= \arg\min_{\boldsymbol{u} \in \mathcal{U}} \boldsymbol{\lambda}^{\mathsf{T}} \boldsymbol{f}(\boldsymbol{x}(t), \boldsymbol{u}, t) \quad \forall t \in [t_0, t_f], \\
\boldsymbol{x}(t_0) &= \boldsymbol{x}_0, \\
\boldsymbol{\lambda}(t_0) &= \boldsymbol{\lambda}_0
\end{aligned} \tag{4}$$

Approved for public release; distribution is unlimited. Public Affairs release approval #AFRL20244796.

where $\boldsymbol{u}^*(t)$ is the input that minimizes the Hamiltonian at time t. This ODE can be solved many times with different random initial costates, $\boldsymbol{\lambda}_0$ to produce an estimate of the boundary of the reachable set. We henceforth refer to this technique of estimating reachaable sets as `ODE`.

Additionally, the initial condition $\boldsymbol{\lambda}(t_0) = \boldsymbol{\lambda}_0$ can be replaced with a final condition $\boldsymbol{\lambda}(t_f) = \boldsymbol{\lambda}_f = -\hat{\boldsymbol{z}}$ which results in a boundary value problem that, under Pontryagin's Maximum Principle, maximizes the final state along $\hat{\boldsymbol{z}}$ [8]. By sampling several final directions, this technique can produce better estimates of the reachable set than simply solving the initial value problem, but comes at the cost of being difficult to solve and requiring more computation time. Moreoever, this technique can be ineffective for reachable sets that are non-convex. By solving the problem with successive alterations to $\hat{\boldsymbol{z}}$ and using previous iterations to kickstart the solution to the current boundary value problem, the technique can be more efficient. We refer to this technique as `BVP`.

Lastly, the boundary value problem can be approximately solved using a technique called `FFOE`, suggested in [15], whereby the dynamics are discretized about a reference trajectory and the costate dynamics are integrated backwards from the final costates to approximate the initial costates.

2.2 Dynamical Systems

2.2.1 Circular, Restricted, Three-Body Problem

To characterize the motion of spacecraft in the cislunar multi-body regime, we employ the circular, restricted, three-body problem (CR3BP) as a simple yet effective means of representing the spacecraft motion. The second-order equations of motion under no external acceleration are given by

$$\begin{aligned} \ddot{\xi} - 2\dot{\eta} &= \xi - \frac{1-\mu}{r_1^3}(\xi+\mu) + \frac{\mu}{r_2^3}(\xi+\mu-1), \\ \ddot{\eta} + 2\dot{\xi} &= \eta - \frac{1-\mu}{r_1^3}\eta - \frac{\mu}{r_2^3}\eta, \\ \ddot{\zeta} &= -\frac{1-\mu}{r_1^3}\zeta - \frac{\mu}{r_2^3}\zeta, \end{aligned} \tag{5}$$

where ξ, η, and ζ represent the Cartesian position of the spacecraft in the rotating synodic frame, and r_1 and r_2 represent the relative distances of the spacecraft to the Earth and Moon, respectively. The gravitational parameter of the system is represented by μ, which depends on the relative masses of the primary bodies. These equations can be equivalently represented as a first-order ordinary differential equation (ODE) $\dot{\boldsymbol{x}}(t) = \boldsymbol{f}(\boldsymbol{x}(t))$, where $\boldsymbol{f} : \mathbb{R}^{n_x} \to \mathbb{R}^{n_x}$ and $n_x = 4$ in the planar case and $n_x = 6$ in the non-planar case.

2.2.2 High-Fidelity Ephemeris Model

For precise study of reachable sets of low-thrust cislunar spacecraft, we employ a high-fidelity ephemeris model. The equations of motion are expressed in the synodic frame and are non-dimensionalized to be analogous to the CR3BP. Ephemeris positions, velocities, accelerations, and jerks of the gravitational bodies are obtained in the J2000 frame about the Solar-System barycenter and are non-dimensionalized. The synodic frame is determined by the ephemeris positions and velocities of the Earth and Moon and its origin is given by the barycenter of the Earth and Moon. The acceleration in this rotating frame, denoted by $\ddot{\boldsymbol{r}}_R$, is given by

$$\ddot{\boldsymbol{r}}_R = -\sum_{i=1}^{n_p} \frac{\mu_i}{\|\boldsymbol{d}_i\|_2^3}\boldsymbol{d}_i - M^\intercal \ddot{M} - 2M^\intercal \dot{M}\dot{\boldsymbol{r}}_R - M^\intercal \ddot{\boldsymbol{R}}_I. \tag{6}$$

Here, $\boldsymbol{R}_I$ is the location of the synodic frame origin in the J2000 frame; M is the direction cosine matrix associated with the synodic rotating frame; $\boldsymbol{d}_i$ is the vector from the ith gravitational body to the spacecraft in the rotating frame, given by $\boldsymbol{d}_i = \boldsymbol{r}_R - M^\intercal(\boldsymbol{r}_i - \boldsymbol{R}_I)$; and, lastly, μ_i is the non-dimensionalized gravitational parameter of the ith body. The quantities $\boldsymbol{R}_I$, M, $\dot{M}$, $\ddot{M}$, and $\boldsymbol{r}_i$ are all obtained from ephemeris data and are therefore purely time varying. Like the CR3BP, these equations of motion can be expressed as a first-order time-varying ODE of the form $\dot{\boldsymbol{x}}(t) = \boldsymbol{f}(\boldsymbol{x}(t), t)$.

2.2.3 Propulsion System

For modeling of the inputs to the system, the equations of motion can be written as

$$\dot{\boldsymbol{x}}(t) = \boldsymbol{f}(\boldsymbol{x}(t),t) + \frac{T_{max}}{m} B\,\boldsymbol{u}(t), \tag{7}$$

where T_{max} represents the maximum thrust of the propulsion system, m denotes the mass of the spacecraft, and $B = [\mathbf{0}_{\frac{n_x}{2}\times\frac{n_x}{2}}, I_{\frac{n_x}{2}\times\frac{n_x}{2}}]^\intercal$. We neglect varying mass due to its negligible impact on the results. Under this system, the input set is given by

$$\mathcal{U} = \{\boldsymbol{u} \mid \|\boldsymbol{u}\|_2 \leq 1\}. \tag{8}$$

2.3 State-Transition Tensors

State-transition tensors (STTs) approximate continuous-time dynamics about a reference trajectory as discrete-time polynomial equations. They have seen use in numerous astrodynamics applications such as orbital guidance [4], uncertainty propagation [14], and stochastic optimal control [6]. In comparison to the state-transition matrix, STTs can produce higher accuracy approximations of deviations from some reference trajectory due to deviations at some earlier time.

Considering an arbitrary ODE, $\dot{\boldsymbol{x}}(t) = \boldsymbol{f}(\boldsymbol{x}(t),t)$, the flow of the system is defined as $\boldsymbol{x}(t) = \phi(t,\boldsymbol{x}(t_0),t_0)$ and satisfies the system's ODEs. The deviation from a trajectory is defined as

$$\delta\boldsymbol{x}(t) \triangleq \phi(t,\boldsymbol{x}(t_0)+\delta\boldsymbol{x}(t_0),t_0) - \phi(t,\boldsymbol{x}(t_0),t_0). \tag{9}$$

Using state-transition tensors, this deviation can be represented analytically with

$$\delta\boldsymbol{x}_i(t) = \sum_{j=1}^{n} \frac{1}{j!}\Phi^{(j)}_{i,n_1\cdots n_j}(t,t_0)\,\delta\boldsymbol{x}_{n_1}(t_0)\cdots\delta\boldsymbol{x}_{n_j}(t_0), \tag{10}$$

where n represents the order of the STT computation and $\Phi^{(j)} \in \mathbb{R}^{\{n_x\}_j}$. Note that Einstein summation convention is used in Equation (10) and subsequent equations; and that with $N = 1$, the state-transition matrix is recovered. For brevity, we henceforth write the tensor multiplication in Equation (10) as $\delta\boldsymbol{x}(t) = \sum_{j=1}^{n}\Phi^{(j)}(t,t_0)\boxtimes\delta\boldsymbol{x}(t_0)$.

The ODEs that characterize the STTs are given up to third-order:

$$\begin{aligned}
\dot{\Phi}_{i,a} &= \boldsymbol{f}^*_{i,\alpha}\Phi_{\alpha,a},\\
\dot{\Phi}_{i,ab} &= \boldsymbol{f}^*_{i,\alpha}\Phi_{\alpha,ab} + f^*_{i,\alpha\beta}\Phi_{\alpha,a}\Phi_{\beta,b},\\
\dot{\Phi}_{i,abc} &= \boldsymbol{f}^*_{i,\alpha}\Phi_{\alpha,abc} + \boldsymbol{f}^*_{i,\alpha\beta}\left(\Phi_{\alpha,a}\Phi_{\beta,bc} + \Phi_{\alpha,ab}\Phi_{\beta,c} + \Phi_{\alpha,ac}\Phi_{\beta,b}\right) + \boldsymbol{f}^*_{i,\alpha\beta\gamma}\Phi_{\alpha,a}\Phi_{\beta,b}\Phi_{\gamma,c},
\end{aligned} \tag{11}$$

where $\boldsymbol{f}^*_{i,n_1\cdots n_k} \triangleq \left.\frac{\partial^k \boldsymbol{f}_i}{\partial\boldsymbol{x}_{n_1}\cdots\partial\boldsymbol{x}_{n_k}}\right|_{x=x^*}$. From some initial state, the STTs can be integrated Equation (11) along with the nominal trajectory to yield the STTs at any arbitrary time points. For more details on STT derivation and application, see [14] and [16].

For a system with inputs, that is with dynamics given by $\dot{\boldsymbol{x}}(t) = \boldsymbol{f}(\boldsymbol{x}(t),\boldsymbol{u}(t),t)$, an augmented state vector can be defined such that $\boldsymbol{z}(t) = [\boldsymbol{x}^\intercal(t),\boldsymbol{u}^\intercal(t)]^\intercal$. Then the augmented dynamics are given by

$$\dot{\boldsymbol{z}}(t) = \boldsymbol{F}(\boldsymbol{z}(t),t) = \begin{bmatrix}\boldsymbol{f}(\boldsymbol{x}(t),\boldsymbol{u}(t),t)\\ \mathbf{0}_{n_u\times 1}\end{bmatrix}. \tag{12}$$

With these augmented dynamics, STTs can be integrated along a grid of time points to reexpress the dynamics in a discrete form. As such, the dynamics with inputs can be represented with STTs as

$$\delta\boldsymbol{x}_i(t_{k+1}) = \sum_{j=1}^{n}\frac{1}{j!}\Phi^{(j)}_{i,n_1\cdots n_j}(t_{k+1},t_k)\,\delta\boldsymbol{z}_{n_1}(t_k)\cdots\delta\boldsymbol{z}_{n_j}(t_k) \iff \delta\boldsymbol{x}(t_{k+1}) = \sum_{j=1}^{n}\frac{1}{j!}\Phi^{(j)}_k\boxtimes\delta\boldsymbol{z}(t_k), \tag{13}$$

Approved for public release; distribution is unlimited. Public Affairs release approval #AFRL20244796.

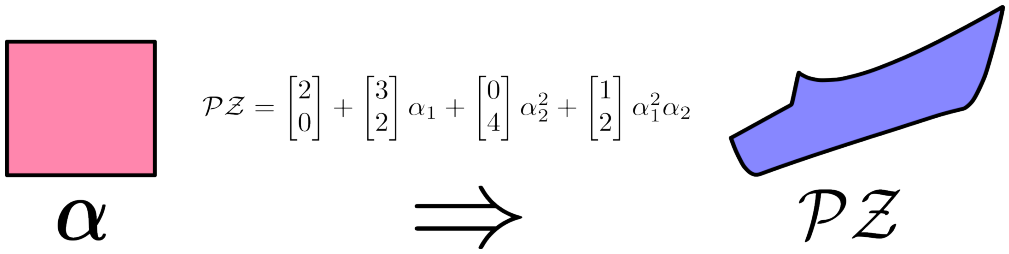

Fig. 1: Visualization of the polynomial zonotope from Equation (15). The unit box is mapped through a polynomial to produce the blue shape, which represents the polynomial zonotope.

where $\Phi_k^{(j)} \in \mathbb{R}^{n_x \times \{n_z\}_{j-1}}$.

State-transition tensor computation time can be significantly improved using a technique that approximates them as so-called directional STTs, proposed in [5]. The technique involves determining the directions of maximum nonlinearity and only propagating these directions, leading to tensors of lower dimensionality such that $\Phi^{(j)} \in \mathbb{R}^{n_x \times n_1 \times \cdots \times n_{j-1}}$. The dimensions of the tensors are either determined heuristically or by analyzing the eigenstructure of the Cauchy-Greene tensor. For more information on the technique, see [5].

2.4 Set-Based Computing and Polynomial Zonotopes

Set-based computing has been used for reachability analysis in several applications, including autonomous driving, robotics, and system biology and involves representing mathematical sets in a computationally tractable manner. Some popular set representations for computing that have been implemented for reachability analysis include ellipsoids, zonotopes, polytopes, and polynomial zonotopes, all of which but the latter are convex representations. Since in nonlinear systems, reachable sets can quickly become non-convex, we make use of sparse polynomial zonotopes [11] to represent reachable sets. We represent polynomial zonotopes, denoted by $\mathcal{PZ}$, with

$$\mathcal{PZ} \triangleq \langle G, E, id \rangle = \left\{ \sum_{i=1}^{h} \left(\prod_{k=1}^{p} \alpha_k^{E_{(k,i)}} \right) G_{(\cdot,i)} \mid \|\alpha\|_\infty \leq 1 \right\}. \tag{14}$$

A polynomial zonotope is characterized by generator matrix $G \in \mathbb{R}^{n \times h}$ and exponent matrix $E \in \mathbb{R}^{p \times h}$. The representation also includes a list identifiers, $id \in \mathbb{R}^p$, which is used to keep track of the dependent factors, $\alpha \in \mathbb{R}^p$.

To demonstrate polynomial zonotopes and their ability to represent unique sets, consider the following example:

$$\mathcal{PZ} = \left\langle \begin{bmatrix}2 & 3 & 0 & 1\\ 0 & 2 & 4 & 2\end{bmatrix}, \begin{bmatrix}0 & 1 & 0 & 2\\ 0 & 0 & 2 & 1\end{bmatrix}, [1,2] \right\rangle = \left\{ \begin{bmatrix}2\\0\end{bmatrix} + \begin{bmatrix}3\\2\end{bmatrix}\alpha_1 + \begin{bmatrix}0\\4\end{bmatrix}\alpha_2^2 + \begin{bmatrix}1\\2\end{bmatrix}\alpha_1^2\alpha_2 \mid \alpha_1, \alpha_2 \in [-1,1] \right\}. \tag{15}$$

The above polynomial zonotope is visualized in Figure 1. Recall that polynomial zonotopes can be used to represent non-convex sets, as can clearly be seen in the visualization.

A polynomial zonotope is closed under several set operations that are relevant for reachability analysis. These relevant set operations, their definitions, and their computation, are as follows: given $\mathcal{PZ}_1 = \langle G_1, E_1, id_1 \rangle$ and $\mathcal{PZ}_2 = \langle G_2, E_2, id_2 \rangle$,

Minkowski Sum:	$\mathcal{PZ}_1 \oplus \mathcal{PZ}_2 \triangleq \{\boldsymbol{s}_1 + \boldsymbol{s}_2 \mid \boldsymbol{s}_1 \in \mathcal{PZ}_1, \boldsymbol{s}_2 \in \mathcal{PZ}_2\} = \langle [G_1, G_2], \text{blkdiag}(E_1, E_2), [id_1, id_2] \rangle$
Linear Map:	$M\mathcal{PZ}_1 \triangleq \{M\boldsymbol{s}_1 \mid \boldsymbol{s}_1 \in \mathcal{PZ}_1\} = \langle MG_1, E_1, id_1 \rangle$
Tensor Map:	$T \boxtimes \mathcal{PZ}_1 \triangleq \{T \boxtimes \boldsymbol{s}_1 \mid \boldsymbol{s}_1 \in \mathcal{PZ}_1\} =$ (See Appendix A)
Cartesian Product:	$\mathcal{PZ}_1 \times \mathcal{PZ}_2 \triangleq \left\{ [\boldsymbol{s}_1^\intercal, \boldsymbol{s}_2^\intercal]^\intercal \mid \boldsymbol{s}_1 \in \mathcal{PZ}_1, \boldsymbol{s}_2 \in \mathcal{PZ}_2 \right\} = \langle \text{blkdiag}(G_1, G_2), \text{blkdiag}(E_1, E_2), [id_1, id_2] \rangle$

For complete proof of the closedness of these operations, see [11]. It should be noted that certain operations, such as the Minkowski Sum and the Cartesian product, can be adjusted in the case of overlapping identifiers, in order to preserve interdependencies between the dependent factors.

Approved for public release; distribution is unlimited. Public Affairs release approval #AFRL20244796.

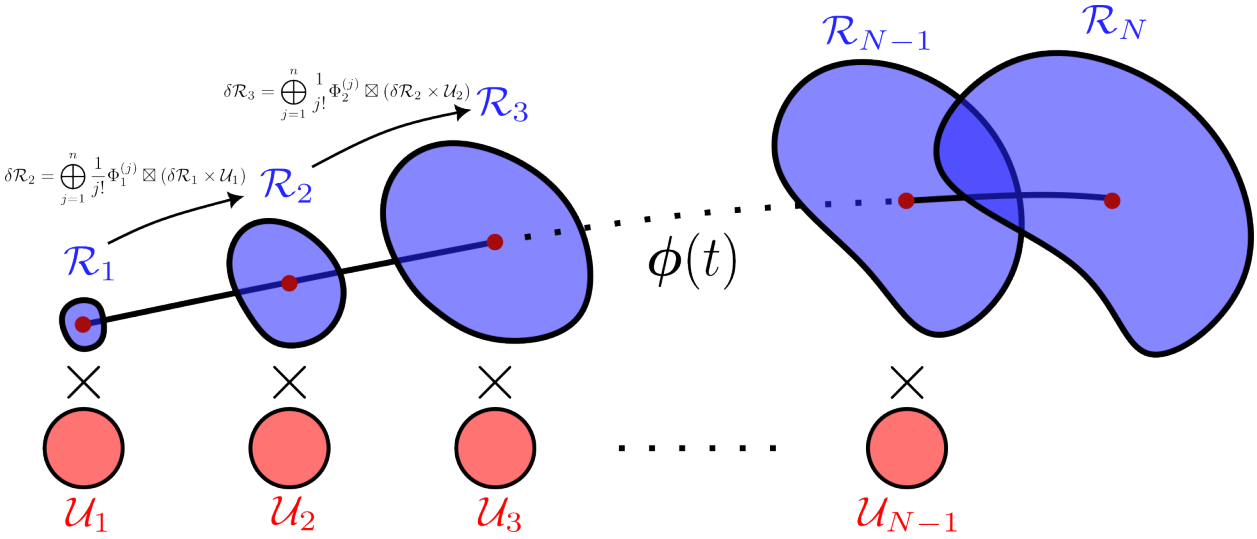

Fig. 2: Visualization of the proposed reachability technique. The polynomial-zonotope reachable sets and input sets can be mapped through the STT-polynomial dynamics.

Many of the above operations increase the dimensionality of the polynomial zonotope. For example, a three-dimenisonal tensor map of a polynomial zonotope with h generators results in a polynomial zonotope with h^2 generators. Repeated operations on a polynomial zonotope will lead to exponential growth in the number of generators. As such, it is necessary to periodically perform reduction to the polynomial zonotope to keep the number of generators at a manageable size. polynomial-zonotope reduction is performed by reducing the order of the zonotope approximated by the weakest generators of the polynomial zonotope. For more information on zonotope and polynomial-zonotope reduction, see [12] and [11]. For reduction, we employ the principle-component analysis (PCA) technique outlined in [12]. The reduction operation of polynomial zonotope to a desired order h_{des} is henceforth denoted by $\texttt{Reduce}(\mathcal{PZ}, h_{des})$.

3. REACHABILITY ALGORITHM

With the background established, we now present the algorithm for propagating polynomial-zonotope reachable sets under STT approximation of the continuous-time dynamics. The reachable set at each time point is defined by $\mathcal{R}_k \triangleq \mathcal{R}(t_k)$. Additionally, the deviated reachable set is given by $\delta\mathcal{R}_k \triangleq \mathcal{R}_k \oplus (-\boldsymbol{\phi}(t_k))$. The input set in polynomial-zonotope form at each time point is given by $\mathcal{U}_k$. This input set can be expressed as a polynomial zonotope using standard conversion techniques. For example, the unit circle input set can be approximated in polynomial-zonotope form with

$$\mathcal{U} = \left\{\boldsymbol{u} \in \mathbb{R}^2 \mid \|\boldsymbol{u}\|_2 \leq 1\right\} \approx \left\langle I_{2\times 2} \otimes \left[1, -\frac{1}{4}, -\frac{1}{32}, -\frac{1}{128}\right], I_{2\times 2} \otimes \mathbf{1}_{1\times 4} + \begin{bmatrix} 0 & 1 \\ 1 & 0 \end{bmatrix} \otimes [0,2,4,6], id_k \right\rangle. \tag{16}$$

Moreover, each input set must have a unique set of identifiers id_k to differentiate it from all other input sets. With these definitions, we see that

$$\left\{[\delta\boldsymbol{x}(t_k)^\intercal, \boldsymbol{u}(t_k)^\intercal]^\intercal \mid \delta\boldsymbol{x}(t_k) \in \delta\mathcal{R}_k, \boldsymbol{u}(t_k) \in \mathcal{U}_k\right\} = \left\{\delta\boldsymbol{z}_k \mid \delta\boldsymbol{z}_k \in \delta\mathcal{Z}_k \triangleq \delta\mathcal{R}_k \times \mathcal{U}_k\right\}. \tag{17}$$

Furthermore, the polynomial zonotope produced by the Cartesian product of $\delta\mathcal{R}_k$ and $\mathcal{U}_k$, $\delta\mathcal{Z}_k$, can be mapped through the STT dynamics in Equation (13) since

$$\left\{\sum_{j=1}^{n} \frac{1}{j!}\Phi_k^{(j)} \boxtimes \delta\boldsymbol{z}_k \mid \delta\boldsymbol{z}_k \in \delta\mathcal{Z}_k\right\} = \left\{\bigoplus_{j=1}^{n} \frac{1}{j!}\Phi_k^{(j)} \boxtimes \delta\mathcal{Z}_k\right\}. \tag{18}$$

Approved for public release; distribution is unlimited. Public Affairs release approval #AFRL20244796.

Algorithm 1 State Transition Tensor Reachable Set Propagation Algorithm

Input Initial State $\boldsymbol{x}_1$, Initial Deviation $\delta\mathcal{R}_1$, Input Set $\mathcal{U}$, Discretization $\{t\}$, STT Order n, Max Generators h_{max}
Output Reachable Set Sequence $\{\mathcal{R}\}$

function STT REACHABILITY
  $\left\{\{\boldsymbol{\phi}\},\{\Phi^{(1)}\},\cdots,\{\Phi^{(n)}\}\right\} \leftarrow$ IVP solution to STT Equation (10) along $\{t\}$ under dynamics $\boldsymbol{f}(\boldsymbol{x},\boldsymbol{u},t)$.
  for $t_k \in \{t\}$ **do**
    $\mathcal{U}_k \leftarrow \mathcal{PZ}(\mathcal{U})$ ▷ Convert input set to polynomial zonotope with unique identifiers
    $\delta\mathcal{Z}_k \leftarrow \delta\mathcal{R}_k \times \mathcal{U}_k$
    $\delta\mathcal{R}_{k+1} \leftarrow \bigoplus_{j=1}^{n} \frac{1}{j!}\Phi_k^{(j)} \boxtimes \delta\mathcal{Z}_k$
    if $h_{k+1} \geq h_{max}$ **then** ▷ Perform Reduction
      `Reduce`$(\delta\mathcal{R}_{k+1}, h_{max})$
    end if
    $\mathcal{R}_{k+1} \leftarrow \delta\mathcal{R}_{k+1} \oplus (\boldsymbol{\phi}(t_{k+1}))$
  end for
end function

Therefore, the following sequence can be applied to propagate reachable sets:

$$\begin{aligned} \delta\mathcal{R}_{k+1} &= \bigoplus_{j=1}^{n} \frac{1}{j!}\Phi_k^{(j)} \boxtimes \delta\mathcal{Z}_k, \\ \mathcal{R}_{k+1} &= \delta\mathcal{R}_{k+1} \oplus (\boldsymbol{\phi}(t_{k+1})). \end{aligned} \tag{19}$$

Under Equation (19), the polynomial-zonotope representations of the reachable set and input set at the current time point undergo a Cartesian product, linear mapping, tensor mapping, and Minkowski summation to produce a polynomial-zonotope representation of the reachable set at the next time point. Since all of these operations are exact, the reachable set at the next time point is exact under the STT dynamics.

However, under this propagation rule, the order of the polynomial zonotopes increases exponentially. If $\mathcal{R}_k$ has h generators, then $\mathcal{R}_{k+1}$ will have $\sum_{j=1}^{n} h^j$ generators. As such, it is necessary to apply order reduction when the polynomial-zonotope order exceeds some threshold, h_{max}. This inevitably leads to some inaccuracy in the propagation since the order-reduction operation will produce slight over-approximations of the polynomial zonotope. The final algorithm is presented in Algorithm 1 and is visualized in Figure 2.

The algorithm includes several tunable parameters that affect the runtime and accuracy of the resulting reachability computation. Increasing the order of the STTs, n, increases the runtime of the STT computation and the set propagation but can provide greater accuracy computation of the reachable sets. Moreover, increasing the maximum generator count, h_{max}, likewise increases the computation time, but can provide greater tightness on the resulting reduced polynomial zonotope.

3.1 Van der Pol Oscillator Example

Algorithm 1 is evaluated for a Van der Pol oscillator system. The reachability problem is given by:

$$\dot{\boldsymbol{x}} = \begin{bmatrix} x_2 \\ (1-x_1^2)x_2 - x_1 + .05u \end{bmatrix}, \mathcal{U} = \{u \mid u \in [-1,1]\}, \quad \boldsymbol{x}_1 = [.5,0]^\intercal, \delta\mathcal{R}_1 = \emptyset, \quad \{t\} = \{0.0,.1,\cdots,3.0\}.$$

The problem is solved with $h_{max} = 200$ and $n = 3$. The runtimes of the operations of the algorithm are listed in Table 1. The resulting sets are visualized in Figure 3 along with 100 extremal trajectories generated using the ODE technique outlined in Section 2.1.

Approved for public release; distribution is unlimited. Public Affairs release approval #AFRL20244796.

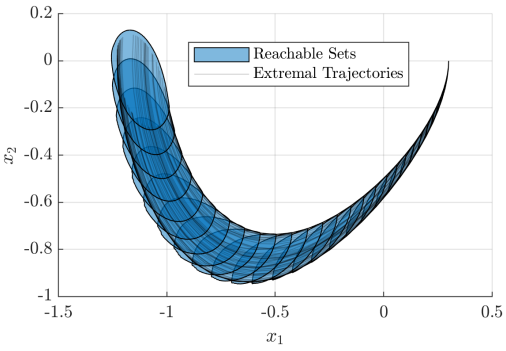

Fig. 3: Reachability solution for Equation (20).

Operation	Evaluations	Total Runtime
STT Generation	1	1.549s
$\delta\mathcal{R}_{k+1} \leftarrow \bigoplus_{j=1}^{n} \Phi_k^{(j)} \boxtimes \delta\mathcal{Z}_k$	30	3.750s
$\texttt{Reduce}(\delta\mathcal{R}_{k+1}, h_{max})$	26	0.478s

Table 1: Runtimes of Algorithm 1 for the Van der Pol system.

In this example, the algorithm produces tight over-approximations of the exact reachable set, which is outlined by the extremal trajectories. The inaccuracy of the computed sets grows in time for two reasons: 1. Repeated reduction of successive polynomial zonotopes leads to inaccuracy over time; and 2. As the reachable set expands, the STT approximation of the dynamics in the vicinity of the reference becomes less accurate. For these reasons the algorithm performs best for short timespans and for problems involving low control authority.

4. REACHABILITY ANALYSIS OF LOW-THRUST, CISLUNAR SPACECRAFT

In this section, we demonstrate the algorithm in two scenarios for low-thrust cislunar spacecraft. Firstly, we compare Algorithm 1 and existing techniques for a spacecraft in a distant retrograde orbit under planar CR3BP dynamics. Secondly, we demonstrate Algorithm 1 for a spacecraft with a close flyby of the moon under ephemeris dynamics.

For the following examples, the following parameters are used for the dynamical system, which are consistent with low-thrust spacecraft in the cislunar system:

Gravitational Parameter	Distance Unit [m]	Time Unit [s]	Maximum Thrust [N]	Spacecraft Mass [kg]
$\mu = .0122$	$DU = 3.825\text{e}8$	$TU = 3.724\text{e}5$	$T_{max} = 1.1\text{e}{-3}$	$m = 14$

Furthermore, for the ephemeris system, we include additional gravitational perturbations from the Sun and Venus. The epoch for the ephemeris simulation is 2024-05-01 12:00:00 TDB.

4.1 Distant Retrograde Orbit Comparison

In this example, we compare several reachability techniques for a distant retrograde orbit (DRO) in the planar CR3BP. The reachability problem is formulated as:

$$\dot{\boldsymbol{x}} = \boldsymbol{f}(\boldsymbol{x}) + \frac{T_{max}}{m} B\boldsymbol{u}, \quad \mathcal{U} = \{\boldsymbol{u} \mid \|\boldsymbol{u}\|_2 \leq 1\}, \quad \boldsymbol{x}_1 = [0.2765, 0.0, 0.0, 2.1379]^\intercal, \, \delta\mathcal{R}_1 = \emptyset, \quad \{t\} = \{0.0, 0.1, \cdots, 3.0\}.$$

The problem is solved with the following methods: 1. Solutions to the IVP in Section 2.1; 2. The Fast First-Order Estimate algorithm (`FFOE`) [15]; 3. Continuous-time BVP [8]; and 4. Algorithm 1. Each method is visuallized in Figure 4. The reachability estimates are projected into the position and velocity space and visualized in Figure 5. The runtimes for each algorithm are found in Table 2 For the three extremal trajectory based methods, 100 trajectories are resolved. Moreover, for the `FFOE` and BVP, samples are taken in the position space as to produce extremal trajectories that maximize distance. For the STT reachability method, we take $n = 2$ and $h_{max} = 400$. Moreover, due to difficulties with ellipsoidal sets, we instead use $\mathcal{U} = [-1, 1]^2$, i.e., the unit box, as the input set. This leads to over-approximation of the reachable set, but tighter approximations than if the unit circle were used.

The final reachability estimates in Figure 5 show that the set propagation results in greater over-approximations than the extremal trajectories.

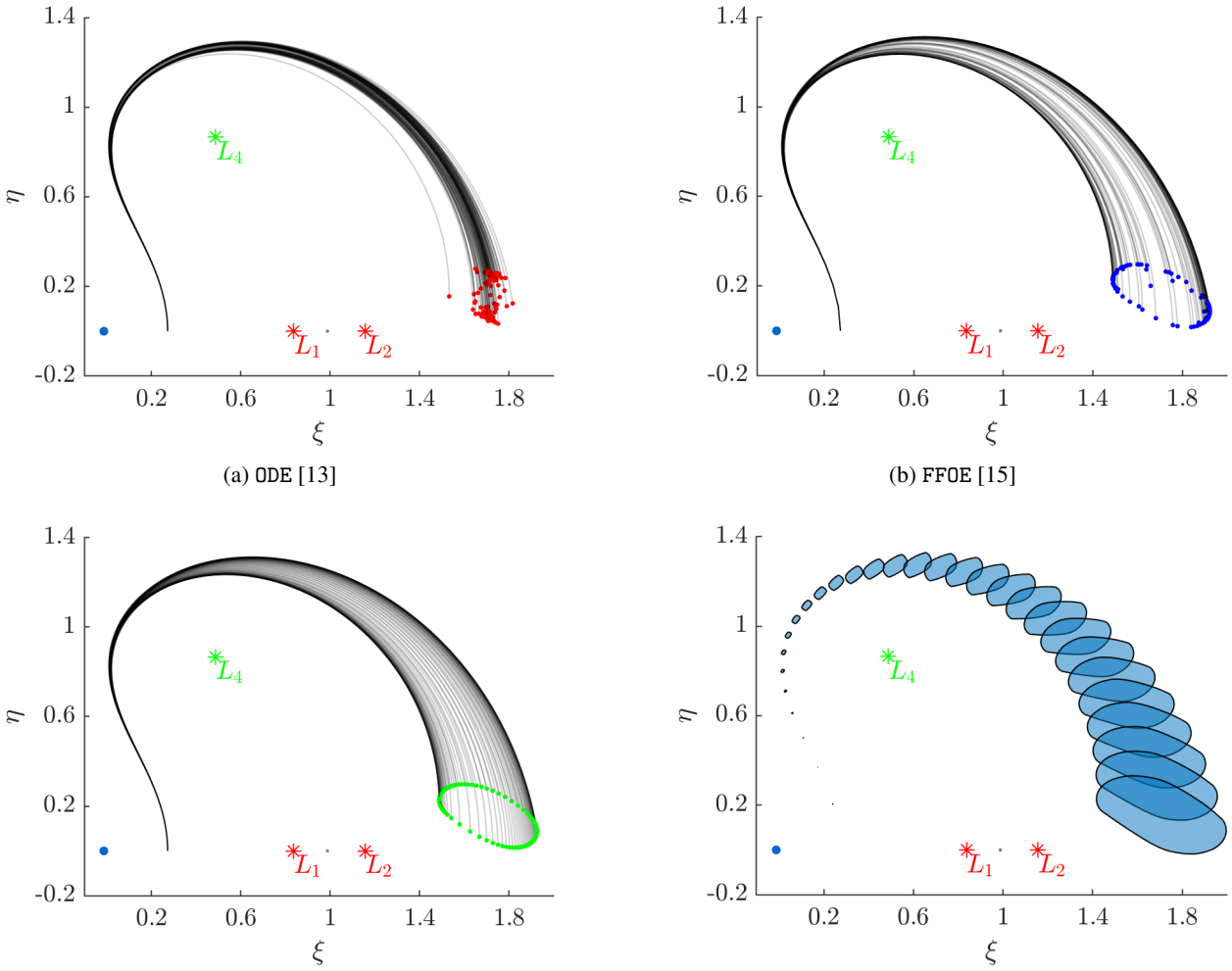

(a) ODE [13]

(b) FFOE [15]

(c) BVP [8]

(d) Algorithm 1

Fig. 4: Low-thrust DRO reachability realizations for various methods.

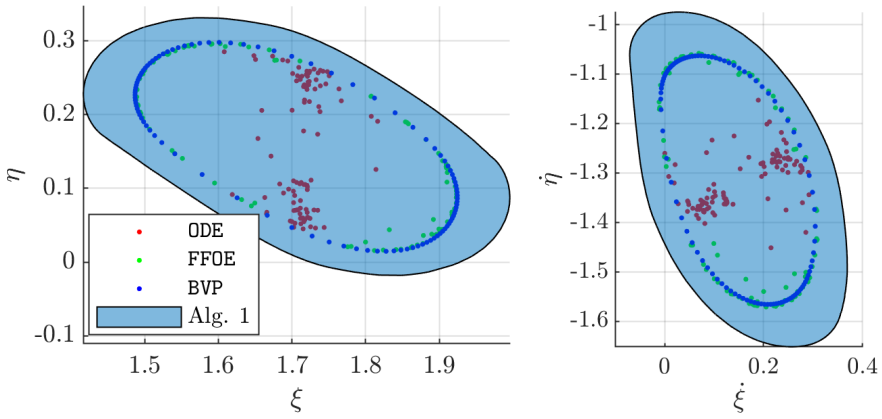

(a) Position reachability projection.

(b) Velocity reachability projection.

Algorithm	Runtime
ODE [13]	4.0389s
FFOE [15]	18.2106s
BVP [8]	16.5983s
Algorithm 1	5.7925s

Table 2: Algorithm Runtimes

Fig. 5: Final DRO reachability estimates.

4.2 Near-Rectilinear Halo Orbit Moon Flyby

In this example, we demonstrate Algorithm 1 for a satellite starting from a near-rectilinear halo orbit under the high-fidelity ephemeris model outlined in Section 2.2.2. The reachability problem is given by:

$$\dot{\boldsymbol{x}} = \boldsymbol{f}(\boldsymbol{x},t) + \frac{T_{max}}{m} B\boldsymbol{u}, \quad \mathcal{U} = \{\boldsymbol{u} \mid \|\boldsymbol{u}\|_2 \leq 1\}, \quad \boldsymbol{x}_1 = [0.91, -0.01, 0.16, 0.03, -0.08, 0.01]^\intercal,$$
$$\delta\mathcal{R}_1 = \emptyset, \qquad \{t\} = \{0.0, 0.05, \cdots, 1.0\}.$$

Algorithm 1 is used with $n = 2$ and $h_{max} = 60$. The resulting sets are projected onto the $x-y$ and $y-z$ planes and can be visualized along with 100 extremal trajectories in Figure 6. The reachable sets are computed in 0.716 seconds.

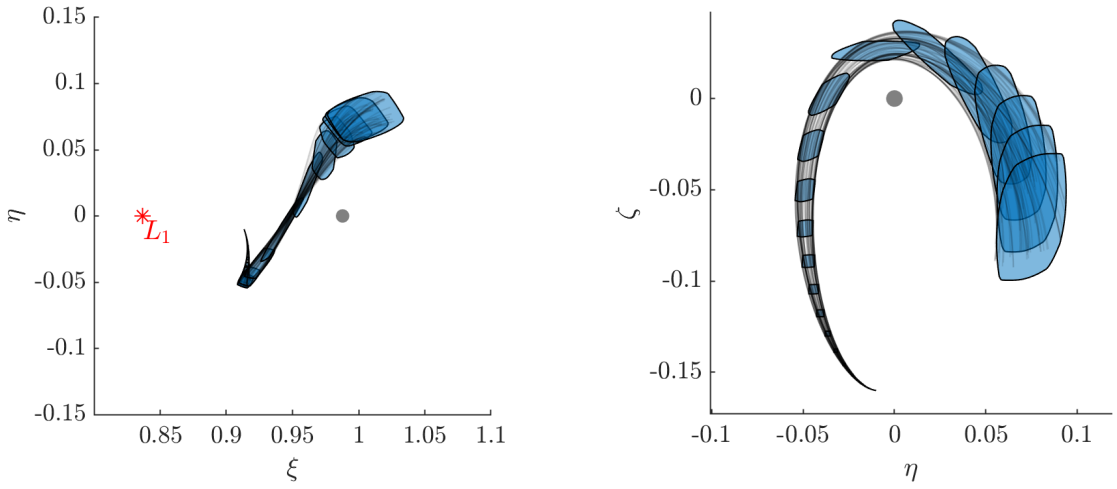

(a) Top position view.

(b) Side position view.

Fig. 6: NRHO Moon flyby reachable sets.

5. DISCUSSION

In both the distant retrograde orbit and near-rectilinear halo orbit examples, the proposed algorithm is able to produce good estimates of the reachable sets with quick computation time. In contrast to techniques that rely on the propagation of a large number of trajectories, the proposed algorithm requires only one numerical integration for the entire reachability computation. This is beneficial for situations in which the numerical integration is computationally intensive, as is the case for high-fidelity propagation. Moreover, we believe that the proposed method is advantageous in that it provides the reachability estimates in a set realization, instead of as a collection of points. The polynomial zonotopes can be converted into polytopes, which can be then be used for evaluating collision regions, visualization, and determining detection regions. Polynomial zonotopes can also represent non-convex sets, which allows for uniform sampling of the boundary of the reachable set.

There exist several key areas of improvement and exploration for the proposed method. Since the STT dynamics are only valid within some region of the reference trajectory, large sets cannot be accurately propagated. Some means of alleviating this issue include incorporating splitting, whereby the polynomial zonotope is split into numerous components and reference trajectories. Additionally, tightness of reachable set can be lost over long propagation times due to repeated order reduction of the polynomial zonotope. Improving the tightness of the reduction step of polynomial zonotopes is therefore an important area for improvement. Lastly, the proposed algorithm provides no guarantees for over or under approximation of the true reachable set. Formulating the problem with STTs to produce these guarantees would be beneficial for safety-critical scenarios.

Approved for public release; distribution is unlimited. Public Affairs release approval #AFRL20244796.

6. CONCLUSION

In this paper, we presented a novel technique for performing reachability analysis for low-thrust cislunar spacecraft. By leveraging state-transition tensors to propagate polynomial zonotopes, reachable sets can be generated about a reference trajectory. Moreover, the technique only requires one numerical integration, in contrast to other popular techniques that rely on the propagation of a large number of trajectories. Because of this, the method lends itself well to reachability computation for high-fidelity, ephemeris models. Additionally, the algorithm produces a continuous set realization of the reachable set, in contrast to existing techniques which rely on the propagation of several trajectories.

Further improvements to the proposed algorithm could involve better methods for polynomial-zonotope order reduction, methods for guaranteeing over-approximation or under-approximation of the reachable set, and reachable tube estimation. Moreover, to the knowledge of the authors, this paper presents the first implementation of set-based computing for SSA applications. The authors believe that extending some of the presented techniques to other key aspects of astrodynamics, such as uncertainty propagation and state estimation, would be a fruitful endeavor.

7. ACKNOWLEDGEMENTS

The authors acknowledge support from the Air Force Research Laboratory and the U.S. Department of the Air Force Summer Faculty Fellowship Program.

8. REFERENCES

[1] M. Althoff. Reachability analysis of nonlinear systems using conservative polynomialization and non-convex sets. In *International Conference on Hybrid Systems: Computation and Control*, 2013.

[2] M. Althoff, G. Frehse, and A. Girard. Set propagation techniques for reachability analysis. *Annual Review of Control, Robotics, and Autonomous Systems*, 4:369–395, 2021.

[3] S. Bansal, M. Chen, S. Herbert, and C. Tomlin. Hamilton-Jacobi reachability: A brief overview and recent advances. In *2017 IEEE 56th Annual Conference on Decision and Control (CDC)*, pages 2242–2253, 2017.

[4] S. Boone and J. McMahon. Rapid local trajectory optimization using higher-order state transition tensors and differential dynamic programming. In *Proceedings of the AAS/AIAA Astrodynamics Specialist Conference*, South Lake Tahoe, CA, Paper AAS20-582, 2020.

[5] S. Boone and J. McMahon. Directional state transition tensors for capturing dominant nonlinear effects in orbital dynamics. *Journal of Guidance, Control, and Dynamics*, 46:431–442, 2023.

[6] M. Fujiwara and R. Funase. Autonomous trajectory guidance under uncertain dynamical environment using state transition tensors. In *Proceedings of the 2022 IEEE Aerospace Conference (AERO)*, Big Sky, MT, 2022.

[7] M. Holzhinger and D. Scheeres. Reachability analysis applied to space situational awareness. In *Advanced Maui Optical and Space Surveillance Technologies Conference (AMOS)*, Maui, HI, 2009.

[8] M. J. Holzinger and D. J. Scheeres. Reachability results for nonlinear systems with ellipsoidal initial sets. *IEEE Transactions on Aerospace and Electronic Systems*, 48:1583–1600, 2012.

[9] R. Jones, D. Curtis, and C. Zagaris. Reachable set approximation in cislunar space with pseudospectral method and homotopy. In *2023 IEEE Aerospace Conference*, pages 1–7, 2023.

[10] N. Kochdumper. *Extensions of Polynomial Zonotopes and their Application to Verification of Cyber-Physical Systems*. PhD thesis, Technical University Munich, 2021.

[11] N. Kochdumper and M. Althoff. Sparse polynomial zonotopes: A novel set representation for reachability analysis. *IEEE Transactions on Automatic Control*, 66:4043–4058, 2020.

[12] A.-K. Kopetzki, B. Schürmann, and M. Althoff. Methods for order reduction of zonotopes. In *Proceedings of the 2017 IEEE 56th Annual Conference on Decision and Control (CDC)*, Melbourne, VIC, Australia, 2017.

[13] T. Lew, R. Bonalli, and M. Pavone. Convex hulls of reachable sets. arXiv:2303.17674, 2024.

[14] R. S. Park and D. J. Scheeres. Nonlinear mapping of Gaussian statistics: Theory and applications to spacecraft trajectory design. *Journal of Guidance, Control, and Dynamics*, 29:1367–1375, 2006.

[15] P. R. Patel and D. J. Scheeres. Rapid and automatic reachability estimation of electric propulsion spacecraft. *The Journal of the Astronautical Sciences*, 70:45 (20 pp.), 2023.

[16] J. Turner, M. Majji, and J. Junkins. High-order state and parameter transition tensor calculations. In *Proceedings of the AIAA/AAS Astrodynamics Specialist Conference and Exhibit*, Honolulu, HI, Paper AIAA-2008-6453, 2008.

A. TENSOR MAP OF A POLYNOMIAL ZONOTOPE

Given a tensor $T \in \mathbb{R}^{n_x \times \{n_k\}_{N-1}}$ with dimension N, the tensor mapping of a polynomial zonotope $\mathcal{PZ} = \langle G, E, id \rangle$ is defined by

$$T \boxtimes \mathcal{PZ} \triangleq \{T \boxtimes \boldsymbol{s} \mid \boldsymbol{s} \in \mathcal{PZ}\}, \tag{20}$$

and can be solved for with

$$T \boxtimes \mathcal{PZ} = \langle \bar{G}, \bar{E}, id \rangle, \tag{21}$$

where

$$\begin{aligned} \bar{G}_{\left(i, h^{N-1}(i_1-1)+\cdots+i_{N-1}\right)} &= T_{i, n_1 \cdots n_{N-1}} G_{n_1, i_1} \cdots G_{n_{N-1}, i_{N-1}}, \\ \bar{E}_{\left(\cdot, h^{N-1}(i_1-1)+\cdots+i_{N-1}\right)} &= \bar{E}_{(\cdot, i_1)} + \cdots + \bar{E}_{(\cdot, i_{N-1})}, \\ i_j &= \{1, \cdots, h\} \; \forall j = \{1, \cdots, N-1\}. \end{aligned} \tag{22}$$

Note that Einstein notation is used in Equation (22) as is used for state-transition tensors.

Approved for public release; distribution is unlimited. Public Affairs release approval #AFRL20244796.